Wind and Structures, *Vol. 31, No. 3 (2020) 241-253*
DOI: https://doi.org/10.12989/was.2020.31.3.241

Parametric optimization of an inerter-based vibration absorber for wind-induced vibration mitigation of a tall building

Qinhua Wang[1,2a], Haoshuai Qiao[1b], Wenji Li*[3], Yugen You[3], Zhun Fan[3,4] and Nayandeep Tiwari[1]

[1]*Department of Civil and Environmental Engineering, Shantou University, Shantou City, Guangdong Province, China*
[2]*Guangdong Engineering Center for Structure Safety and Health Monitoring, Shantou University, Shantou 515063, China*
[3]*Department of Electronic and Information Engineering, Shantou University, Shantou City, Guangdong Province, China*
[4]*Key Lab of Digital Signal and Image Processing of Guangdong Province, Shantou University, 515063, Guangdong, China*

(*Received August 2, 2019, Revised August 2, 2020, Accepted August 4, 2020*)

Abstract. The inerter-based vibration absorber (IVA) is an enhanced variation of Tuned Mass Damper (TMD). The parametric optimization of absorbers in the previous research mainly considered only two decision variables, namely frequency ratio and damping ratio, and aimed to minimize peak displacement and acceleration individually under the excitation of the across-wind load. This paper extends these efforts by minimizing two conflicting objectives simultaneously, i.e., the extreme displacement and acceleration at the top floor, under the constraint of the physical mass. Six decision variables are optimized by adopting a constrained multi-objective evolutionary algorithm (CMOEA), i.e., NSGA-II, under fluctuating across- and along-wind loads, respectively. After obtaining a set of optimal individuals, a decision-making approach is employed to select one solution which corresponds to a Tuned Mass Damper Inerter/Tuned Inerter Damper (TMDI/TID). The optimization procedure is applied to parametric optimization of TMDI/TID installed in a 340-meter-high building under wind loads. The case study indicates that the optimally-designed TID outperforms TMDI and TMD in terms of wind-induced vibration mitigation under different wind directions, and the better results are obtained by the CMOEA than those optimized by other formulae. The optimal TID is proven to be robust against variations in the mass and damping of the host structure, and mitigation effects on acceleration responses are observed to be better than displacement control under different wind directions.

Keywords: inerter-based vibration absorber; multi-objective evolutionary algorithm; decision-making approach; wind-induced vibration; high-rise buildings

1. Introduction

In recent decades, the development of technology and materials in the field of civil engineering leads to an enormous increase in the construction rate of high-rise buildings. Slender high-rise buildings with flexible nature and less damping are sensitive to fluctuating wind loads (Kareem *et al.* 1999), which leads to large displacement and acceleration responses (Simiu and Scanlan 1986). To mitigate the wind-induced vibrations and satisfy the occupants' comfort criteria, different kinds of passive control devices were proposed, e.g., Tuned Mass Damper (TMD) (Ormondroyd and Den Hartog 1928, Kari 1979, Iban *et al.* 2013, Rezaee and Aly 2016), Multi Tuned Mass Damper (MTMD) (Poovarodom *et al.* 2001, Poovarodom *et al.* 2002, Poovarodom *et al.* 2003, Ubertini 2010, Zhou *et al.* 2015) and Tuned Liquid Column Damper (TLCD) (Min *et al.* 2005, Diana *et al.* 2013, Di Matteo *et al.* 2017, Di Matteo *et al.* 2018). Some conventional mathematical methods based on the gradient analysis of objective functions (Warburton 1982) and intelligent algorithms (e.g., Genetic Algorithm (Poh'Sie *et al.* 2016) and Particle Swarm Algorithm (LEUNG *et al.* 2009) were adopted to optimize the three parameters (including mass, frequency and damping ratio) of a TMD. To further alleviate enormous mass of TMD installed on high-rise buildings, IVAs (such as TMDI and TID) were proposed as enhanced variants of the TMD due to the "mass amplification" effect of inerter (Lazar *et al.* 2014, Marian and Giaralis 2015).

It is evident from previous researches that optimization plays an important role in enhancing the performance of TMDI/TID to seismic design. Lazar *et al.* (2014) proposed a TID tuning strategy for structural vibration suppression based on the Den Hartog's TMD tuning guidelines, i.e., fixed-point theory. The superiority of the TID was verified by analyzing the seismic performance of the optimally-tuned TMD and TID for multi-storey structures. Dario *et al.* (2018) performed the displacement-oriented constrained optimization of a TID on a base-isolated structure by adopting the built-in MATLAB® "fmincon" function to seek the optimal values of frequency and damping ratio. Marian and Giaralis (2015) classified both TMD and TID as special cases of the TMDI and carried out a preliminary optimization of a TMDI installed on a single-degree-of-freedom (SDOF) structure under white-noise excitation to

*Corresponding author, Ph.D.
E-mail: wenji_li@126.com
[a]Associate Professor
E-mail: qinhuawang@stu.edu.cn
[b]Ph.D. Student
E-mail: haoshuaiqiao@foxmail.com

http://www.techno-press.com/journals/was&subpage=7
ISSN: 1226-6116 (Print), 1598-6225 (Online)

minimize the variance of displacement by solving two partial differential equations of objective functions. Furthermore, they employed the “min-max” constraint optimization algorithm to optimize a support-excited chain-like MDOF system to minimize displacement responses under earthquake action. Giaralis and Taflanidis (2018) optimized the design variables of a TMDI including frequency, damping and inertance ratio by taking the objective function as a linear combination of floor accelerations, inter-storey drifts, and attached mass displacement of a linear MDOF system excited by seismic excitation. A nonlinear global optimization algorithm was employed, and the results demonstrated that the TMDI can suppress higher modes of vibration as compared to a TMD. Through a numerical search algorithm, Dario and Ricciardi (2017) fixed effective mass ratio and performed the optimization of frequency and damping ratio for a base isolation multistory structures under seismic excitation. The same algorithm was also adopted by Dario and Ricciardi (2018) to carry out the optimization of four different performance indices (i.e., displacement performance index, acceleration performance index, filtered energy index, and TMDI stroke index) of a TMDI for structures with nonlinear base isolation systems.

In addition to earthquake action, slender high-rise buildings are also sensitive to fluctuating wind loads (Simiu and Scanlan 1986). In the past few years, it has been found that the IVAs can usually provide better performance in mitigating wind-induced vibrations than other traditional control devices such as TMD, which catches the attention of several researchers. For example, Giaralis and Petrini (2017a) studied the wind-induced vibration mitigation effect of TMDI on a 74-storey steel frame building of 305m height. Some gains were achieved in reducing peak displacement and acceleration at the top floor compared to a TMD. In their research, Warburton Tuning formulae (Warburton 1982) were extended to obtain reasonable but non-optimal parameters of a TMDI. A parametric study for a TMDI with fixed mass ratio and increasing inertance coefficient ratio was performed. To further improve the efficiency of a TMDI in controlling wind-induced vibrations, Giaralis and Petrini(2017b) optimized the parameters of a TMDI installed on the same structure. The components of wind force were modeled by a power spectral density (PSD) matrix. A pattern search algorithm was used to optimize the frequency ratio and damping ratio for fixed values of mass ratio and inertance ratio, which aims to minimize the hourly extreme acceleration of the top floor. Lastly, the closed-form expressions of optimal frequency ratio and damping ratio as functions of mass ratio and inertance ratio were obtained by employing polynomial fitting. Wang *et al.* (2019) concluded that TID can provides better vibration mitigation effects than TMD and TMDI with the same physical mass ratio under aerodynamic loads obtained from the wind tunnel test of a benchmark tall building. The optimization of the frequency ratio, damping ratio, and floor index of TMDI/TID with other three parameters fixed (i.e., mass ratio, inertance ratio, and topologies of inerter) was performed. The results indicated that by installing a TMDI/TID in the lower storey rather than the top floor results in a much better mitigation in extreme displacement and acceleration responses.

This work extents the previous researches on investigation of wind-induced vibration control using IVAs in the following aspects: (i) Unlike the single objective performance-based optimizations performed in previous researches, the optimization of IVAs aims to optimize two conflicting objectives simultaneously, namely displacement and acceleration responses, and a practical concern, i.e., the device mass, is considered to be a constraint, (ii) based on a real case and its wind tunnel test, the optimization under along- and across- wind excitation is performed, (iii) the excitation- and structure-dependent features of IVA are investigated by carrying out robustness analyses. With these three main novelties, in this paper, the parameters of an IVA installed in a benchmark building are optimized by adopting NSGA-II considering two objectives, i.e., wind-induced displacement and acceleration responses. Once the Pareto front (PF) of IVAs is obtained, a decision-making approach is adopted to choose one representative solution. Then this solution is compared with previous results (Giaralis and Petrini 2017a, 2017b). To validate the robustness of the optimally-tuned TID achieved by the suggested method, responses of TID-equipped structure under different wind directions and perturbations of structural properties are evaluated.

2. Background theory

2.1 Numerical simulation procedure

A high-rise building equipped with a TMDI can be simplified as a lumped-mass model as shown in Fig.1. The motion equation of this TMDI-equipped building under wind loads can be expressed as below

$$\left[M\right]\left\{\ddot{D}(t)\right\}+\left[C\right]\left\{\dot{D}(t)\right\}+\left[K\right]\left\{D(t)\right\}=\left\{P(t)\right\} \tag{1}$$

where, $\{\ddot{D}(t)\}$, $\{\dot{D}(t)$, $\{D(t)\}$ are vectors of acceleration, velocity, and displacement of each lumped mass at arbitrary time t, respectively. $\{P(t)\}$ is the vector of aerodynamic forces at arbitrary time t obtained from multi-point synchronized pressure wind-tunnel tests. When a TMDI is installed at the t^{th} floor with a “-p” topology, the matrices of mass, damping, and stiffness can be written as follows (Wang *et al*. 2019)

$$\begin{aligned}
\left[M\right]&=\left[M\right]_s^{n+1}+\left(m_{\mathrm{TMDI}}+b\right)\mathbf{1}_{\mathbf{n+1}}\mathbf{1}_{\mathbf{n+1}}^{T}+b\mathbf{1}_{\mathbf{t\text{-}p}}\mathbf{1}_{\mathbf{t\text{-}p}}^{T}-b\left(\mathbf{1}_{\mathbf{n+1}}\mathbf{1}_{\mathbf{t\text{-}p}}^{T}+\mathbf{1}_{\mathbf{t\text{-}p}}\mathbf{1}_{\mathbf{n+1}}^{T}\right)\\
[C]&=[C]_s^{n+1}+c_{\mathrm{TMDI}}\left(\mathbf{1}_{\mathbf{n+1}}\mathbf{1}_{\mathbf{n+1}}^{T}+\mathbf{1}_{\mathbf{t}}\mathbf{1}_{\mathbf{t}}^{T}-\mathbf{1}_{\mathbf{n+1}}\mathbf{1}_{\mathbf{t}}^{T}-\mathbf{1}_{\mathbf{t}}\mathbf{1}_{\mathbf{n+1}}^{T}\right)\\
\left[K\right]&=\left[K\right]_s^{n+1}+k_{\mathrm{TMDI}}\left(\mathbf{1}_{\mathbf{n+1}}\mathbf{1}_{\mathbf{n+1}}^{T}+\mathbf{1}_{\mathbf{t}}\mathbf{1}_{\mathbf{t}}^{T}-\mathbf{1}_{\mathbf{n+1}}\mathbf{1}_{\mathbf{t}}^{T}-\mathbf{1}_{\mathbf{t}}\mathbf{1}_{\mathbf{n+1}}^{T}\right)
\end{aligned} \tag{2}$$

where $[M]_s^{n+1}$, C_s^{n+1}, K_s^{n+1} $\epsilon \mathrm{R}^{(n+1)\mathrm{x}(n+1)}$ are the mass, damping, and stiffness matrices augmented by one last (bottom) row with zero entries and one last (rightmost) column of zero entries in the original matrices. m_{TMDI}, c_{TMDI} and k_{TMDI} are the attached mass, damping of the dashpot elements, and the stiffness of the linear spring, respectively. The b is the inertance coefficient of the inerter. The first

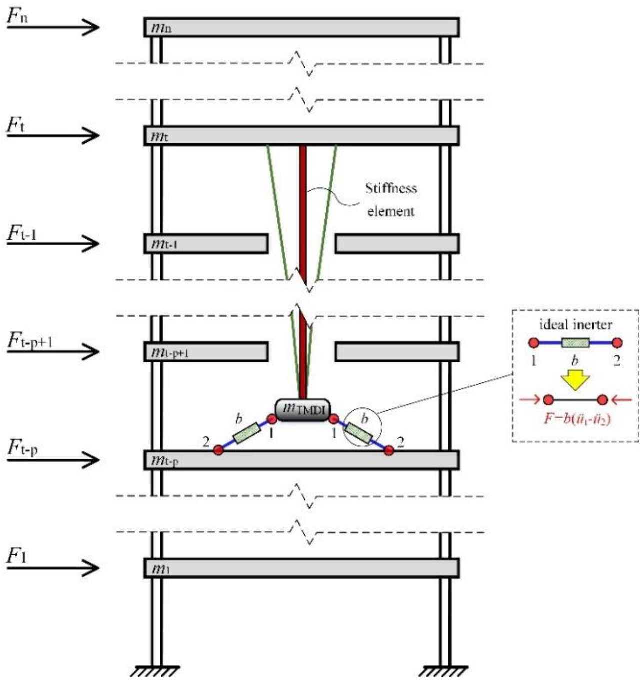

Fig. 1 A lumped mass model of a TMDI equipped a structure with "-*p*" topologies (Wang *et al*. 2019)

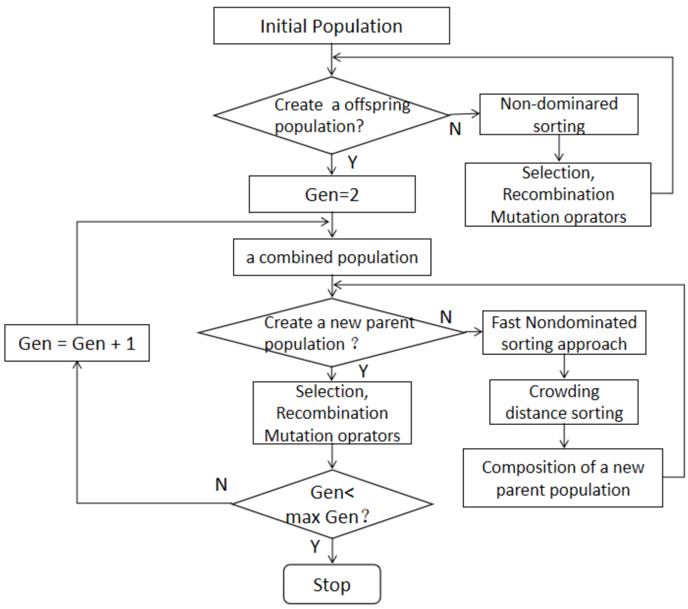

Fig. 2 The flowchart of NSGA-II

terminal of the inerter is connected to the attached mass of the TMDI and the second terminal of the inerter is attached to the $(t\text{-}p)^{th}$ floor. Only the $(t\text{-}p)^{th}$ entry of the vector $1_{t\text{-}p} \epsilon R^{(n+1)x1}$ is equal to one, while all the other entries are equal to zeros. The superscript T indicates a transpose operator. Noteworthy, the equations of motion of a TMD- and TID-equipped building can be retrieved from Eq. (1) by setting the attached mass and inertance values to zeros in Eq. (2), respectively.

Once the wind-induced vibration equation of a TMDI-equipped high-rise building is established, the numerical time-stepping method, i.e., Newmark-β algorithm (M. Newmark 1959), is adopted to calculate wind-induced displacement and acceleration responses at the top floor according to Eq. (1). Further, NSGA-II is adopted as the optimization algorithm to determine the optimal parameters of the TMDI.

2.2 Theory of NSGA-II

After formulating the optimization problem for the TMDI-equipped structure with six decision variables and two conflicting objectives, a widely used CMOEA, i.e., NSGA-II (Deb 2002), is adopted to solve the formulated constrained multi-objective optimization problem (CMOP). The flowchart of NSGA-II is shown in Fig. 2.

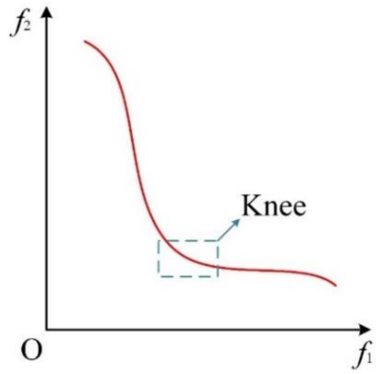

Fig. 3 A simple Pareto optimal front with a knee point

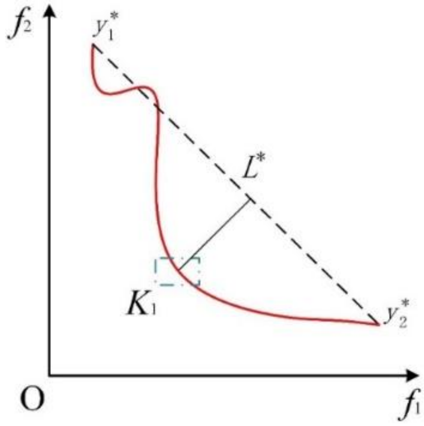

Fig. 4 A "knee" K_1 of a Pareto front as characterized

Table 1 Main dynamic parameters of the primary structure (Wang *et al*. 2019)

Total mass M (dead and live loads)	First-order natural frequency along x-axis	First-order generalized mass	First-order damping ratio ζ_{s1}
231659 t	0.176 Hz	61287 t	1%

2.3 Theory of decision-making approaches

To select a suitable solution from the entire PF, a concept of the knee point is employed. In the region around the knee point, a small change exerted to one of the objectives on the PF will result in a large effect on at least one other objective (Cai *et al*. 2016). For example, a simple PF is described in Fig. 3, which has two objectives to be minimized. This PF has a clearly visible bump in the middle, which is called a "knee". Without any preference in advance, the knee is a widely used solution for decision makers in multi-objective optimization.

A knee point of a PF is found by solving the following nonlinear programming problem (Zitzler and Künzli 2004)

$$\max_{x\in PS} dist\Big(F(x), L\big(F(x_1^*), F(x_2^*)\big)\Big) \tag{3}$$

where x represents the decision variables of a solution, PS is the Pareto optimal set, and F is the objective function. $x_i^* \in \arg\min_{x\in PS} f_i(x), i=1,2$. The characteristics of the knee point can be interpreted as the maximum expansion of the curve with respect to the line $L\big(F(x_1^*), F(x_2^*)\big)$ containing the two extreme points (y_1^* and y_2^*) of the curve as shown in Fig. 4. Since we are interested in "convex bumps" (see Fig. 3, or the references (Zitzler and Künzli 2004, Beume *et al*. 2007), we define the distance of the $F(x)$ a candidate solution to $L\big(F(x_1^*), F(x_2^*)\big)$ as follows

$$D(x, x_1^*, x_2^*) = \begin{cases} dist\Big(F(x), L\big(F(x_1^*), F(x_2^*)\big)\Big)\, if\ \ f_2(x) \le g\big(f_1(x)\big) \\ -dist\Big(F(x), L\big(F(x_1^*), F(x_2^*)\big)\Big)\, else \end{cases} \tag{4}$$

where $g(x)=L\big(F(x_1^*), F(x_2^*)\big)$. Using this function, we can modify the nonlinear programming problem in Eq. (3) by

$$\max_{x\in PS} D(x, x_1^*, x_2^*) \tag{5}$$

3. Case study

3.1 Benchmark building and wind tunnel test

The benchmark building has a height of 340 m with 69 floors. As the 58th floor is the topmost floor where the residents live, the installation floor of the IVA is chosen to be lower than 59th floor. The main dynamic parameters of the original structure extracted from a finite element model are listed in Table 1.

Wind tunnel tests of synchronous multiple-point pressure measurement for the building were carried out in the boundary layer wind tunnel under 24 wind directions (as shown in Fig. 5). The coordinates of structural analysis and the wind direction definition are shown in Fig. 6. It can be seen that the incoming winds at 0° and 270° wind directions (denoted as β_w) are the least affected by surrounding buildings, which correspond to the along- and across-wind, respectively. The x-axis components of the aerodynamic forces at each floor are obtained in terms of scale technique of the wind tunnel tests. The further details about the dynamic characteristics of the original structure and wind tunnel tests can be referred to Ref. (Wang *et al*. 2019).

$$\mu_{\mathrm{TMDI}} = \frac{m_{\mathrm{TMDI}}}{M} \tag{6}$$

where M is the total mass of the original structure. In practice, the mass ratio of a super-high rise building rarely exceeds 0.5% (Giaralis and Petrini 2017a). The analysis of vibration mitigation effect of a TMDI installed on the same benchmark building in reference (Wang *et al*. 2019) was carried out with $\mu_{\mathrm{TMDI}} = 0.25\%$. A slightly wider interval of mass ratio, i.e., [0%,0.5%], is adopted in the present study.

The inertance coefficient ratio β, is defined as in Eq. (7), with value in the range [0,1] (Giaralis and Petrini

Table 2 The configuration of NSGA-II

Parameters	Value
Maximum generation	1000
Population size	200
Crossover probability	0.9
Mutation probability	1/6
The number of decision variables	6

2017a).

$$\beta = \frac{b}{M} \tag{7}$$

The frequency ratio υ_{TMDI} is denoted as

$$\upsilon_{\text{TMDI}} = \frac{\omega_{\text{TMDI}}}{\omega_1} = \sqrt{\frac{k_{\text{TMDI}}}{m_{\text{TMDI}} + b}} / \omega_1 \tag{8}$$

where ω_{TMDI} is the free vibration frequency of TMDI, and ω_1 is the first order frequency of the original structure. Giaralis and Petrini (2017b) indicated that the optimal frequency ratio slightly less than 1 has the most efficient vibration mitigation effect. Considering the uncertainty effect of newly added parameters (t and $-p$) on the optimization, the frequency ratio is limited in the following range [0.7,1.2].

The damping ratio ζ_{TMDI} is constrained within [0, 20%] which has a more feasible physical realization based on previous works (Giaralis and Petrini 2017b). It is defined as follow:

$$\zeta_{\text{TMDI}} = \frac{c_{\text{TMDI}}}{2\sqrt{(m_{\text{TMDI}} + b)k_{\text{TMDI}}}} \tag{9}$$

The floor of TMDI installation t and the topologies "$-p$" have been defined in Eq. (2). To further study the mitigation effect of the TMDI, the value of t is set in the range [30,58]. The topology "$-p$" is constrained within [-4,0] with the consideration of the possibilities of implementation and the effect of larger $|-p|$ value in achieving the better vibration mitigation effect of a TMDI (Giaralis and Petrini 2017a).

Once the six parameters are determined, Eq. (1) can be established in terms of aerodynamic forces from wind tunnel tests and be solved by employing numerical time-stepping methods (M. Newmark 1959). Then the two objective (extreme acceleration and displacement responses) can be calculated by $\hat{D}_{acc}=g\sigma_{acc}$ and $\hat{D}_{dis}=\mu_{dis}\pm g\sigma_{dis}$, respectively, where μ_{dis} is the mean displacement, g=3.5 is the peak factor estimated from the empirical formula(Davenport 1964), and σ is the mean square root of corresponding responses. To achieve a good balance between the performance of the TMDI on controlling wind-induced vibrations and its weight which relates to the cost of installation, a constraint on the physical mass of TMDI is set to represent for the secondary economic concern. It was found that the ratios of inertance coefficient over the physical mass of inerter can reach 200 (Papageorgiou and Smith 2006). Thus, the physical mass ratio $\mu=(m_{attachedmass}+m_{inerter})/M=\mu_{\text{TMDI}}+\beta/200$ is adopted to represent for the actual mass of TMDI devices and is determined to be constrained within 0.5%. Under this setting of μ_p, two cases, i.e., TMD (μ_{TMD}=0.5%, $\beta=0$) and TID (μ_{TMD}=0, $\beta=1$), will be included. From stated above, a CMOP can be formulated as follows:

$$\begin{cases} \text{minimize} & f_1(\mu_{\text{TMDI}}, \beta, \upsilon_{\text{TMDI}}, \zeta_{\text{TMDI}}, t, p) = \hat{D}_{acc} \\ & f_2(\mu_{\text{TMDI}}, \beta, \upsilon_{\text{TMDI}}, \zeta_{\text{TMDI}}, t, p) = \left|\hat{D}_{dis}\right| \\ s.t. & \mu_{\text{TMDI}} + \beta / 200 \le 0.5\%, \\ & \mu_{\text{TMDI}} \in [0, 0.5\%], \beta \in [0,1], \\ & \upsilon_{\text{TMDI}} \in [0.7, 1.2], \zeta_{\text{TMDI}} \in [0, 20\%], \\ & t \in [30,58], -p \in [-4,0] \end{cases} \tag{10}$$

where f_1 and f_2 are the two objective functions with six decision variables.

3.3 Optimization results and verification

The parameters of the TMDI installed in the high-rise building are respectively optimized under across- and along-wind fluctuating loads by multi-objective optimization theory. The configuration of NSGA-II is listed in Table 2.

To compare the results of optimization with previous researches, Giaralis tuning formulae (Giaralis and Petrini 2017b) and Warburton tuning formulae (Warburton 1982) are used as listed in Eq. (11) and Eq. (12), respectively.

$$\begin{cases} \upsilon_{\text{TMDI}} = \mu_{\text{TMDI}}\left(\frac{26}{84}\beta - \frac{288}{84}\right) - \frac{1}{84}\beta + 1 \\ \zeta_{\text{TMDI}} = 11\mu_{\text{TMDI}}\left(\beta - \sqrt{\beta} + 1\right) + \frac{11}{65} + \zeta_{s1} \end{cases} \tag{11}$$

where ζ_{s1} is the first modal damping ratio of the original structure.

$$\begin{cases} \upsilon_{\text{TMDI}} = \frac{\sqrt{1 + 0.5(\beta + \mu_{\text{TMDI}})}}{1 + \beta + \mu_{\text{TMDI}}} \\ \zeta_{\text{TMDI}} = \sqrt{\frac{(\beta + \mu_{\text{TMDI}})\left[1 + 0.75(\beta + \mu_{\text{TMDI}})\right]}{4(1 + \beta + \mu_{\text{TMDI}})\left[1 + 0.5(\beta + \mu_{\text{TMDI}})\right]}} \end{cases} \tag{12}$$

3.3.1 Optimization results under across-wind fluctuating loads (270° wind direction)

Due to the vortex shedding, the power spectral density (PSD) of aerodynamic forces at across-wind direction shown in Fig. 7 has a notable peak around dimensionless frequency fB/U(z)=0.06, where f is the frequency in Hz, B is the windward width of the benchmark building, and U(z) is the mean wind velocity at the height of z(m) corresponding to 50 years return period. It can be seen that the frequency components of fluctuating forces based on wind tunnel tests distribute different from the PSD simulated by empirical formulae (Liang *et al*. 2002) due to the surrounding buildings. The PSD of aerodynamic loads

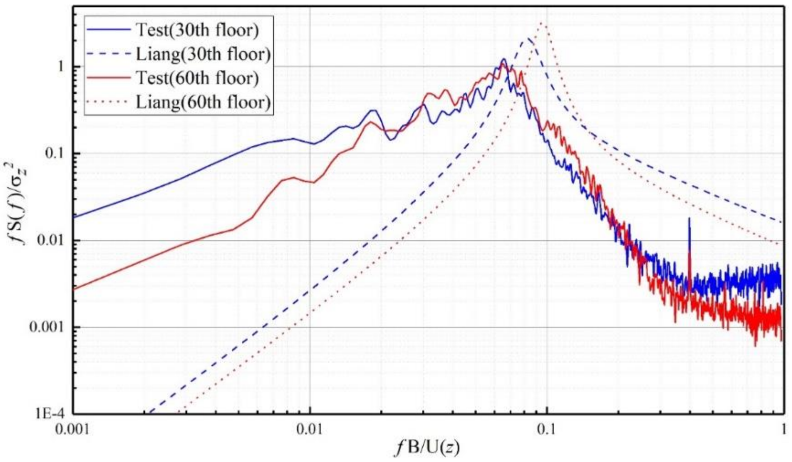

Fig. 7 Power spectrum densities of aerodynamic forces at 270° wind direction

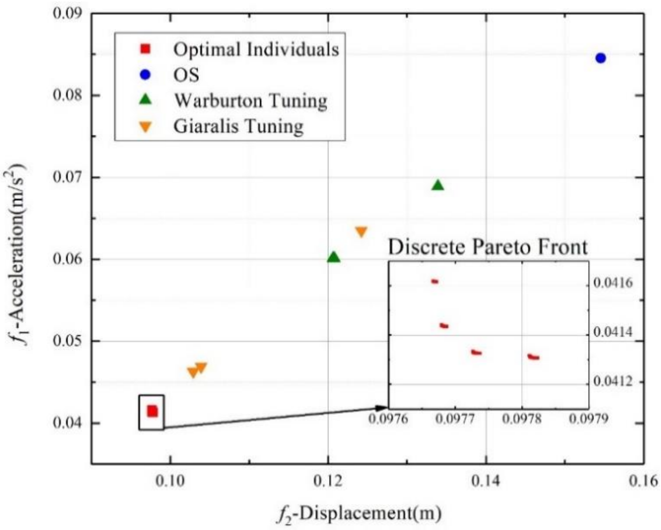

Fig. 8 The PF obtained by NSGA-II at the wind direction 270°

at across-wind indicates a narrow band stochastic process, which is different from the PSD of along-wind fluctuating force indicating a broadband process as shown in Fig. 11.

The optimization results (shown in Fig.8) under across-wind excitation are illustrated in the form of Pareto front. The horizontal axis and vertical axis represent two objects, i.e. extreme displacement and acceleration responses at the top floor, respectively.

Under the constraint of physical mass ratio, the optimal mass ratio and inertance coefficient ratio are equal to 0 and 1 respectively, which indicates that the TID has better mitigation effects than those of the TMDI and TMD. Each point in the PF as shown in Fig. 8 represents a set of optimal parameters of a TID. The PF composes of 200 solutions of optimal parameters and approaches to lower left corner in Fig. 8, which indicates that the optimal parameters in the PF are better than those tuned by Giaralis formulae (Giaralis and Petrini 2017b) and Warburton formulae (Warburton 1982). The obtained PF is in form of curve instead of straight line pointing towards the origin, which indicates that the two objectives, namely extreme displacement and acceleration responses, are conflicting with each other. In addition, the PF obtained under across-wind excitation in Fig. 8 is apparently different from that as shown in Fig. 12 under along-wind loads. It may be attributed to the difference between the spectra of across- and along-wind fluctuating forces, i.e. the spectra of across and along-wind forces are narrow (shown in Fig. 7) and broad band (shown in Fig. 11) stochastic process, respectively.

Generally, each solution in the PF can be used as a design of the TID. For practical application, only one set of the optimal parameters will be selected. According to Eq. (3), a knee point in the PF is selected, which represents the optimal parameters of a TID. Three sets of optimal parameters of TID (selected from the PF), namely minimum extreme displacement (Dis_{min}), acceleration (Acc_{min}) and the knee point respectively, and six more sets of parameters of TID tuned by using Eqs. (11) and (12) are listed in Table 3 for the comparison. The extreme displacement and acceleration of the original structure are also listed in Table 3 to estimate the vibration mitigation effects of the TID with different parameters.

From Table 3, it can be seen that the optimal TID design corresponding to the knee point has a good trade-off of mitigation effects between wind induced displacement and

Table 3 Parameters of optimal TID, TID under Warburton tuning and Giaralis tuning at the wind direction of 270°

Case	Property	μ_{TMDI}	β	υ_{TMDI}	ζ_{TMDI}	t	$-p$	$\hat{D}_{dis}$ (m)	$\hat{D}_{acc}$ (m/s^2)
TID (Pareto Fronts)	Dis_{min}	0	1	1.14	14.2%	42	-4	0.0977	0.0416
	Knee point	0	1	1.16	15.0%	44	-4	0.0977	0.0413
	Acc_{min}	0	1	1.16	15.8%	45	-4	0.0978	0.0413
TID (Warburton Tuning)	Dis_{min}	0	1	0.61	38.2%	42	-4	0.1206	0.0601
	Acc_{min}	0	1	0.61	38.2%	45	-4	0.1208	0.0601
	Conventional case	0	1	0.61	38.2%	58	-4	0.1339	0.0689
TID (Giaralis Tuning)	Dis_{min}	0	1	0.99	17.9%	42	-4	0.1029	0.0463
	Acc_{min}	0	1	0.99	17.9%	45	-4	0.1039	0.0469
	Conventional case	0	1	0.99	17.9%	58	-4	0.1242	0.0635
Original Structure (OS)	\	\	\	\	\	\	\	0.1546	0.0845

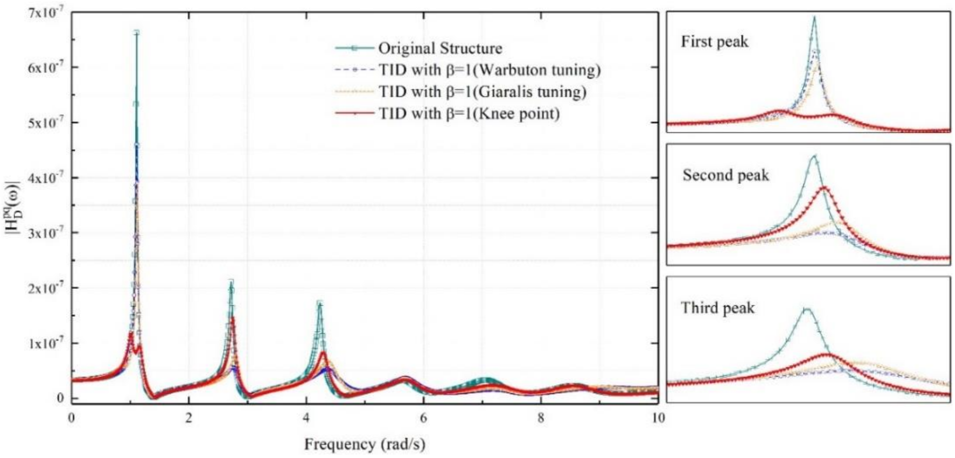

(a)Displacement transfer functions of top floor of the benchmark building

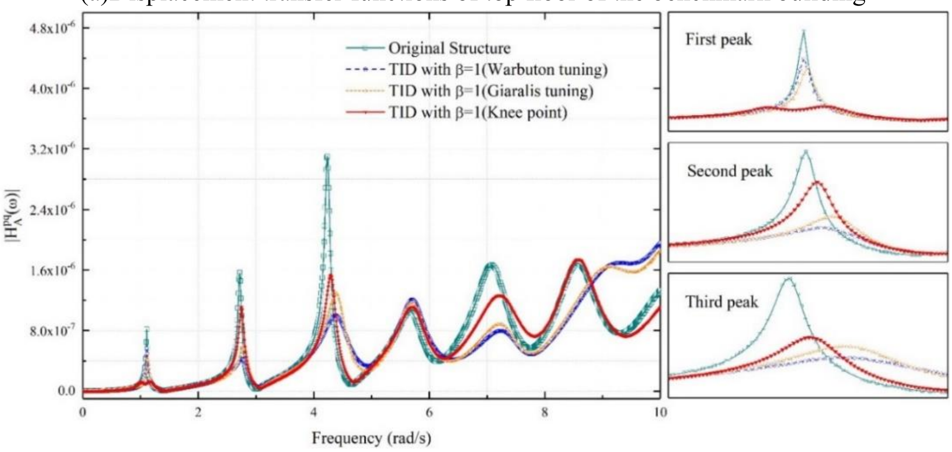

(b)Acceleration transfer functions of top floor of the benchmark building

Fig. 9 Transfer functions of OS and different TID-equipped structures

acceleration responses. TID tuned by Giaralis formulae (Giaralis and Petrini 2017b) can achieve the same vibration mitigation effect as that obtained by NSGA-II, only if the installation floor of TID in eighth and ninth rows in Table 3 are set to be the same as those from NSGA-II. It is worth noted that NSGA-II can simultaneously optimize six parameters, while the formulae (Warburton 1982, Giaralis and Petrini 2017a) can only optimize frequency and damping ratio with the other four parameters of the TMDI fixed.

The comparison among the 200 solutions of optimal parameters in the PF shows that the optimal topologies of TIDs reach the lower bound, i.e., -4. This result of better vibration mitigation effect of TMDIs achieved by the inerter spanning more stories matches well with the previous works (Giaralis and Petrini 2017a, Giaralis and Taflanidis 2018).

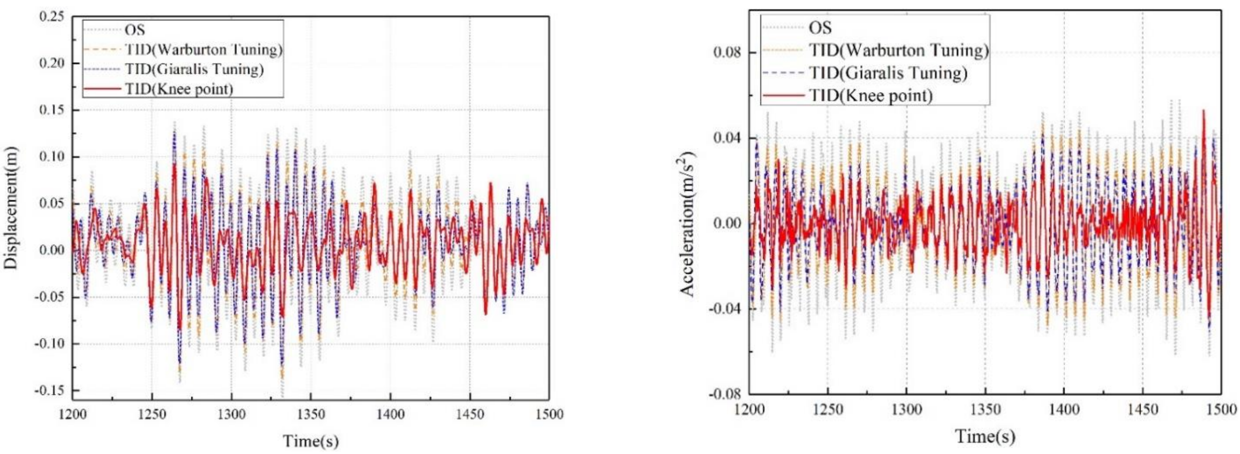

(a) Displacement responses (b) Acceleration responses

Fig. 10 Time histories of (a) displacement and (b) acceleration at the 69th storey corresponding to 270° wind direction

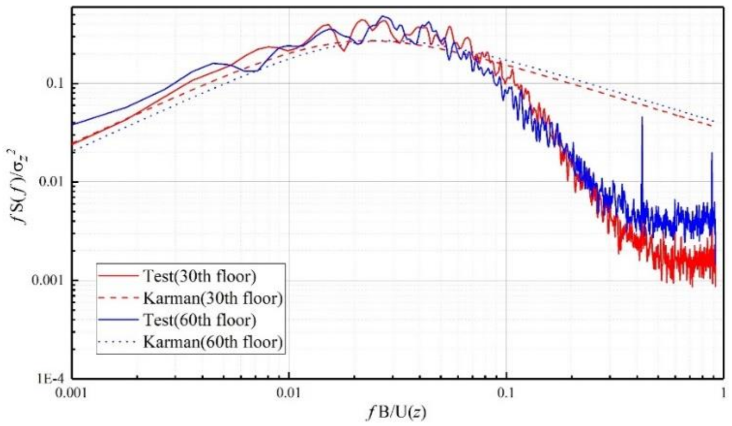

Fig. 11 Power spectrum densities of aerodynamic forces at wind directions of 0°

Besides the parameters mentioned above, the other three parameters, i.e., frequency ratio, damping ratio and TMDI installation floor, have been obtained. The damping ratio increases from 14.2% to 15.8% gradually with the increasing frequency ratio and the TMDI installation floor index. This range of optimal damping ratio is close to the value obtained by Giaralis formulae (Giaralis and Petrini 2017b) but much lower than that mentioned in previous studies for seismic design (Marian and Giaralis 2015, Giaralis and Taflanidis 2018). The optimal frequency ratio in the present case is around 1.15, which approaches to the first natural frequency of the benchmark high-rise building and is close to the optimal frequency ratio in the reference (Giaralis and Petrini 2017b). The optimization results indicate that the TID installed on the upper middle part of the structure (namely 42nd to 45th floor) can provide better vibration mitigation effect rather than that on the top floor.

To verify the optimal parameters of the TID, transfer functions and time histories of displacement and acceleration at top floor are analyzed. Figs. 9(a)-9(b) show the modulus of the transfer function of displacement and acceleration responses, respectively, at the 69th DOF (top floor) of the benchmark building induced by forces at the 69th DOF.

In Fig. 9(a), the first peak appears around the first natural frequency (1.10 rad/s). The first three peaks of the original structure (in dark cyan) are obviously higher than those of the TID-equipped structures, which indicates the efficiency of the TID in vibration control. The parameters of the TID obtained from the knee point can mostly reduce wind-induced displacement responses corresponding to the first vibration mode among the three cases. The results are consistent with those in Table 3. In Fig. 9(b), the highest peak of the acceleration transfer function is observed around the third natural frequency. TIDs efficiently suppress wind-induced acceleration responses corresponding to the first three natural frequencies of the structure. However, as energy of aerodynamic force at 270° wind direction distributes mainly under 1 rad/s (as displayed in Fig. 7), the contribution from first order vibration mode still dominates the acceleration responses.

In time domain analyses, Fig. 10 represents segments of the time-history responses of displacement and acceleration (for a duration of 20 minutes) at the top floor corresponding to 270° wind direction. It is well observed that the best vibration mitigation effect is achieved by the optimal TID for both displacement and acceleration, which is consistent with the results shown in Fig. 9 and Table 3.

3.3.2 Optimization results for along-wind excitation (0° wind direction)

Considering the fact that frequency components of loads

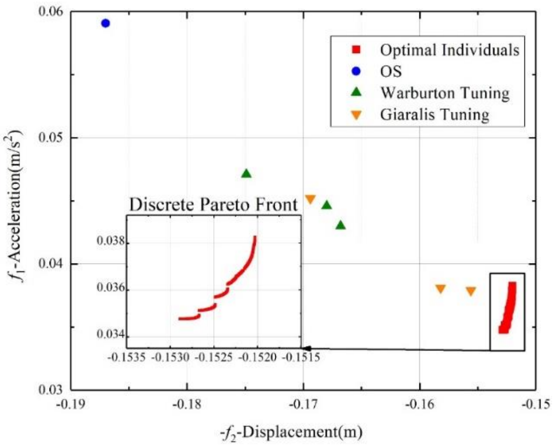

Fig. 12 The PF of the optimization results corresponding to 0°

Table 4 Parameters of optimal TID, TID under Warburton tuning and Giaralis tuning at the wind direction of 0°

Case	Property	μ_{TMDI}	β	υ_{TMDI}	ζ_{TMDI}	t	$-p$	$\hat{D}_{dis}$ (m)	$\hat{D}_{acc}$ (m/s^2)
TID (Pareto Fronts)	Dis_{min}	0	1	1.14	13.3%	42	-4	-0.1520	0.0383
	Knee point	0	1	1.19	15.8%	48	-4	-0.1525	0.0353
	Acc_{min}	0	1	1.19	19.4%	49	-4	-0.1529	0.0348
TID (Warburton Tuning)	Dis_{min}	0	1	0.61	38.2%	42	-4	-0.1668	0.0430
	Acc_{min}	0	1	0.61	38.2%	49	-4	-0.1680	0.0446
	Conventional case	0	1	0.61	38.2%	58	-4	-0.1749	0.0471
TID (Giaralis Tuning)	Dis_{min}	0	1	0.99	17.9%	42	-4	-0.1556	0.0379
	Acc_{min}	0	1	0.99	17.9%	49	-4	-0.1582	0.0381
	Conventional case	0	1	0.99	17.9%	58	-4	-0.1694	0.0452
Original Structure (OS)	\	\	\	\	\	\	\	-0.1870	0.0591

may affect optimal parameters, the optimization under along-wind excitation is also performed. The along-wind force spectra at the 30th and the 60th floor from wind tunnel tests and the along-wind speed spectra following Karman formulae (Von Kármán 1948) are presented in Fig. 11. As the along-wind aerodynamic force is a quasi-steady process, the PSD of along-wind speed may reflect the energy distribution of along-wind force in the frequency domain. In the low frequency range, the PSD from Karman formulae has a good agreement with that from the wind tunnel test. By comparing the PSD of along-wind excitation to that of across-wind excitation as shown in Fig. 7, it is clear that the PSD of along-wind is a broadband stochastic process.

Under the along-wind excitation, TIDs still have better mitigation effects than those of TMDIs and TMDs with the same physical mass ratio. The PF under along-wind excitation is shown in Fig. 12. The trend of PF is almost perpendicular to horizontal axis, which indicates that the displacement mitigation effects among optimal TIDs are almost the same, while the acceleration mitigation effects vary relatively larger among different individuals.

The optimal parameters and wind-induced responses of TMDIs with different tuning formulae are listed in Table 4.

Similar to the optimization results under across-wind excitation, the values of three parameters, i.e., μ_{TMDI}, β and p, have reached the preset bounds. The distribution of the first two parameters indicates that the TID can achieve the best vibration mitigation effect comparing to the TMDI and TMD. The optimal values of the topologies prove that the more stories the inerter span, the better vibration mitigation effect of the TID can be achieved under along-wind excitation. As for the optimal values of other three parameters, a better mitigation effect in displacement responses and a less reduction in acceleration responses are achieved as the three parameters increase simultaneously in their corresponding optimal intervals. By comparing optimal individuals under along-wind excitation with TIDs tuned by Warburton and Giaralis formulae, the same results can be also observed as those under across-wind.

4. Robustness analysis of the optimal parameters of the TID and practical design considerations

4.1 Robustness of the optimally designed TID

Because the optimization of the TID is performed under specific wind excitation and structural properties, it is necessary to investigate the robustness of TID under general condition, i.e., different wind directions and various

Table 5 Parameters of the selected optimal TID

Parameters	Value
Mass ratio	0
Inertance coefficient ratio	1
Frequency ratio	1.17
Damping ratio	15%
Topologies of inerter	4
Floor of TMDI installation	46

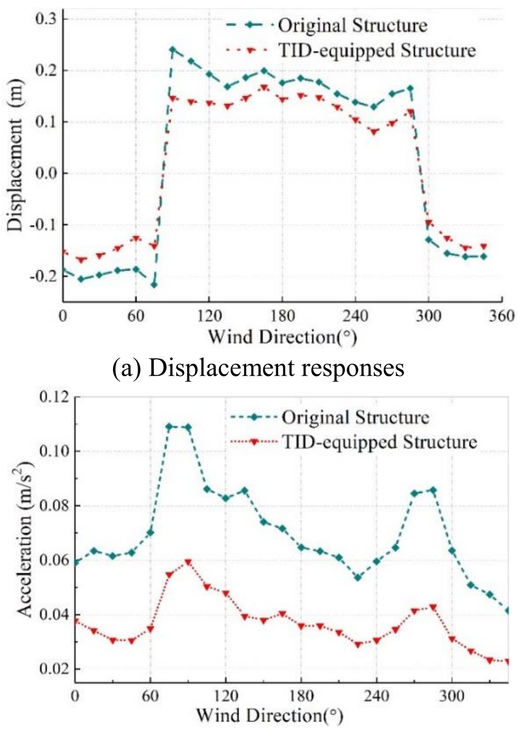

(a) Displacement responses

(b) Acceleration responses

Fig. 13 Wind induced (a) displacement (b) acceleration responses of original structure and TID-equipped structure at 24 wind directions

structural dynamic characteristics. Based on two knee points mentioned in Section 3.3, a group of optimal parameters of TID is selected (denoted as TID_{opt}) and listed in Table 5.

4.1.1 Impacts of different wind directions on the performance of the optimal TID

To investigate the robustness of the optimal TID under different wind directions, displacement and acceleration responses induced by aerodynamic loads under 24 wind directions are calculated and plotted in Fig.13.

In Figs. 13(a) and 13(b), TID_{opt} decreases the extreme displacement and acceleration at top floor of the benchmark building at all 24 wind directions.

To quantify the vibration mitigation effect of the TID, vibration-absorbing factor F_{va} is expressed as below (Wang *et al*. 2019)

$$F_{va} = \left| \frac{R_{\mathrm{OS}} - R_{\mathrm{TID}}}{R_{\mathrm{TID}}} \right| \tag{13}$$

where R_{os} and R_{TID} represent the responses (displacement or acceleration) of the original structure and the TID-equipped structure, respectively. The F_{va} of $\mathrm{TID_{opt}}$ on displacement varies from 39.2% at wind direction of 90° to 10.9% at wind direction of 330°. As compared to the mitigation effect of $\mathrm{TID_{opt}}$ on extreme displacement, larger and more stable reduction on extreme acceleration from 36.2% to 53.9% is achieved. The above discussion indicates that $\mathrm{TID_{opt}}$ has significant robustness in mitigating acceleration at different wind directions.

4.1.2 Impacts of variations of structural dynamic characteristics on the performance of the TID

In addition, the dynamic characteristics of structures may have an impact on the optimization results. In this respect, considering the lumped mass of each DOF, especially live loads, probably change during its service life, the variation range of mass of each floor is set to be [0.9,1.1] times of its original value. Meanwhile, due to the great uncertainty in the estimation of damping (Spence and Kareem 2013), a wider range of [0.8,1.2] times of original values of the damping matrix is determined to represent the perturbation of the damping between stories.

To quantify the vibration mitigation effect of $\mathrm{TID_{opt}}$ under different conditions, a normalized performance index (denoted as *PI*) is defined as below

$$PI = \frac{F_{va}}{F_{va-opt}} \tag{14}$$

where $F_{va\text{-}opt}$ is the vibration-absorbing factor of $\mathrm{TID_{opt}}$ under excitations at wind direction of 270° (36.8% for displacement and 51.0% for acceleration).

Fig. 14 shows the *PI* for displacement and acceleration of the $\mathrm{TID_{opt}}$ equipped structure. The values of *PI* for displacement and acceleration are found to be around 1, which indicates the high robustness of optimal TID against perturbations on structural dynamic properties. A valley at about M/M_{OS}=0.96 in Fig. 14(a) can be observed, which means that variation of mass within [-4%,0%] will weaken the performance of the optimal TID in terms of displacement mitigation. For acceleration *PI* shown in Fig. 14(b), the two valleys occur below M/M_{OS}=0.90 and at M/M_{OS}=1.06, which have the similar trend as shown in Fig. 14(a). The *PI* for both displacement and acceleration decrease gradually with the increase in damping. It may be attributed to the fact that the host structure with larger damping will dissipate more energy. Comparing the extreme values of *PI* in Figs. 14(a) and 14(b), the robustness of the TID in mitigating acceleration is better than that in controlling displacement.

4.2 Practical design considerations of an absorber

It is important to evaluate the implementation difficulty of the optimal parameters of the TID in terms of the stroke of the TID and the inerter force. The root mean square (RMS) of the relative displacement between the two terminals of an inerter is related to the stroke of the inerter. The stroke of the optimally-designed TMD is evaluated by

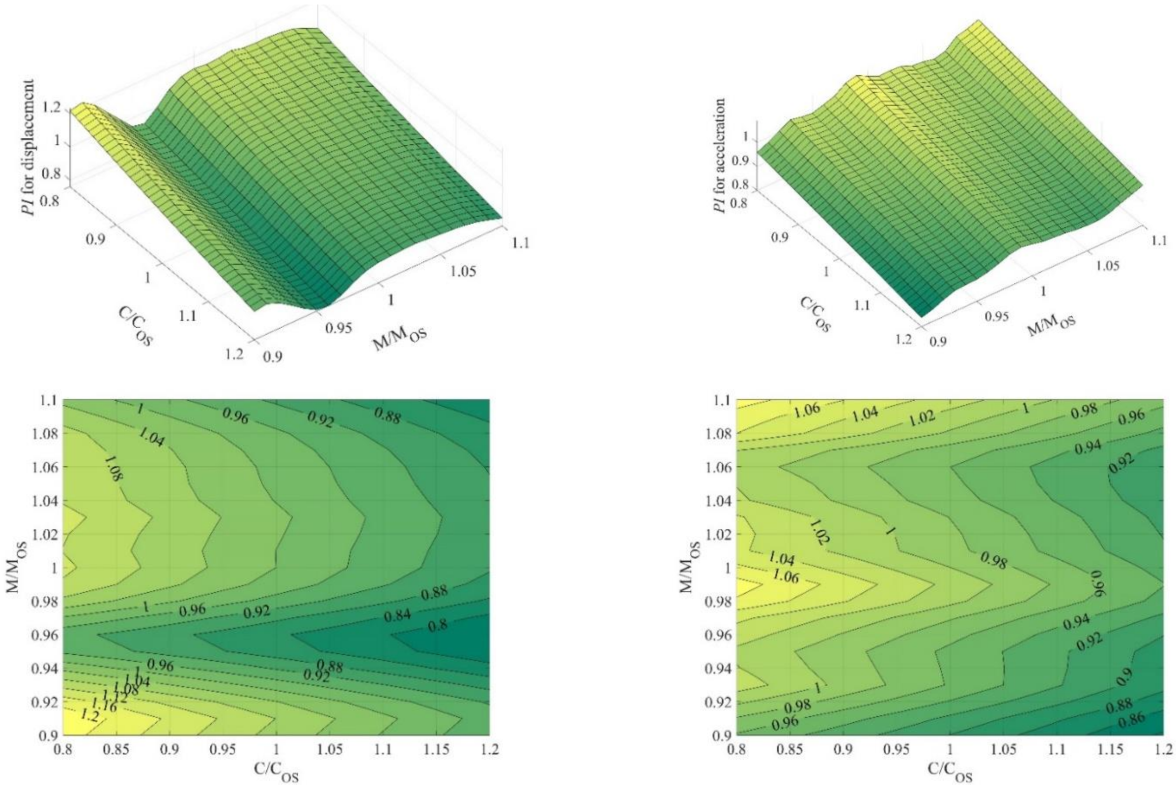

(a) Displacement responses (b) Acceleration responses

Fig. 14 *PI* for (a) extreme displacement and (b) extreme acceleration of TID_{opt} at wind direction of 270° under variations of mass and damping of benchmark building

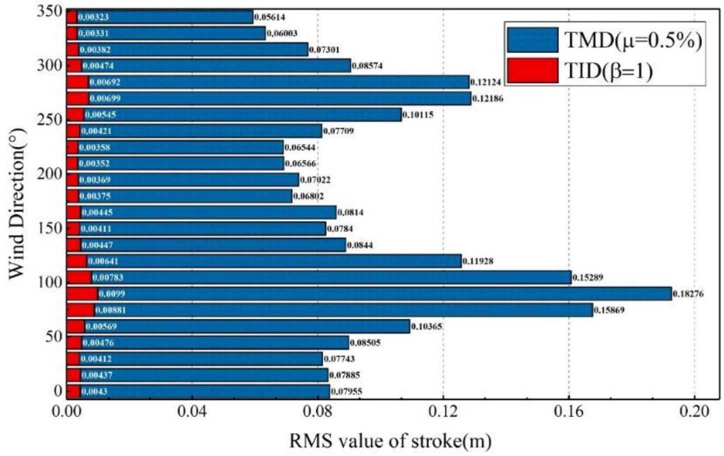

Fig. 15 Root mean square of the TMD and TID stroke

the RMS value of the relative displacement between the attached mass and the optimal installation floor in this case (58^{th} floor). They are calculated at 24 wind directions, and the results are plotted in Fig. 15. Comparing the TID and the TMD with the same physical mass ratio, the inerter can significantly decrease the stroke of the vibration absorbing devices.

The extreme inerter force can be calculated by multiplying inertance coefficient with extreme relative acceleration between its two terminals (Giaralis and Petrini 2017a). The extreme relative acceleration is calculated by Eq. (1), and the corresponding extreme inertance force is 4043kN. According to results reported by Karavasilis *et. al.* (2012), such requirements for inerter force can be implemented safely by adopting several parallel inerters.

5. Conclusions

The parametric optimization of IVAs, i.e., TMDIs and TIDs, is performed by applying NSGA-II to a high-rise building installed with an absorber. The PFs are obtained under across- and along-wind excitations, respectively. Two representative individuals from two discrete PFs are selected by a decision-making approach. The main conclusions of the present work can be summarized as follows:

• The analysis of parameters indicates that the TID can achieve better wind-induced vibration mitigation effects than that of the TMDI and TMD in terms of two optimal objectives, i.e., extreme displacement and acceleration responses. The optimal damping ratio varies from 13% to 19%. The optimal frequency ratio ranged from 1.14 to 1.19. As for the inertance ratio and topologies of inerter, it can be seen that the values have reached the boundaries of their constrained intervals under both types of wind excitations, and the results agree well with the previous researches.

• The case study shows that the TID at the knee point can achieve maximum reduction for both extreme displacement and acceleration of 36.8% and 51.0% at across-wind direction, respectively. The corresponding F_{va} values are 18.7% and 36.2% under along-wind excitation, respectively.

• The acceleration mitigation effect of TID_{opt} is robust under the variation of aerodynamic loads for wind directions ranging from 0° to 345°. For displacement responses, reduction ratios range from 10.9% to 39.2% at different wind directions. In comparison, larger and more stable reduction ratios on extreme acceleration from 36.2% to 53.9% are observed. The TID_{opt} also has a good robustness in engineering application under the variation of dynamic characteristics of the structure. With ±10% and ±20% perturbations exerted on the mass and damping of the original structure, respectively, no significant decrease on values of *PI* is observed.

Future Work

The results in section 4.1.2 indicate that the dynamic properties have significant influences on the performance of IVAs. Thus, further research will focus on the parametric optimization of IVAs with the consideration of the dynamic properties of host structures.

Acknowledgements

Support for this work is provided in part by the National Natural Science Foundation of China (51208291) This support is gratefully acknowledged.

References

Beume, N., Naujoks, B. and Emmerich, M. (2007), “SMS-EMOA: Multiobjective selection based on dominated hypervolume”, *Eur. J. Oper. Res.*, **181**(3), 1653-1669. https://doi.org/10.1016/j.ejor.2006.08.008.

Cai, X., Yang, Z., Fan, Z. and Zhang, Q. (2016), “Decomposition-based-sorting and angle-based-selection for evolutionary multiobjective and many-objective optimization”, *IEEE Trans. Cybern.*, **47**(9), 1-14. https://doi.org/10.1109/TCYB.2016.2586191.

Davenport, A.G. (1964), “Note on the random distribution of the largest value of a random function with application to gust loading”, *Proc. Inst. Civil Eng.*, **28**(2), 187-196. https://doi.org/10.1680/iicep.1964.10112.

De Domenico, D. and Ricciardi, G. (2017), “An enhanced base isolation system equipped with optimal tuned mass damper inerter (TMDI)”, *Earthq. Eng. Struct. Dyn.*, **47**(5), 1169-1192. https://doi.org/10.1002/eqe.3011.

De Domenico, D. and Ricciardi, G. (2018), “Optimal design and seismic performance of tuned mass damper inerter (TMDI) for structures with nonlinear base isolation systems”, *Earthq. Eng. Struct. Dyn.*, **47**(12), 2539-2560. https://doi.org/10.1002/eqe.3098.

De Domenico, D., Impollonia, N. and Ricciardi, G. (2018), “Soil-dependent optimum design of a new passive vibration control system combining seismic base isolation with tuned inerter damper”, *Soil Dyn. Earthq. Eng.*, **105**, 37-53. https://doi.org/10.1016/j.soildyn.2017.11.023.

Deb, K. (2002), “A fast elitist multi-objective genetic algorithm: NSGA-II”, *IEEE Trans. Evol*., **6** 182-197.

Di Matteo, A., Furtmueller, T., Adam, C. and Pirrotta, A. (2018), “Optimal design of tuned liquid column dampers for seismic response control of base-isolated structures”, *Acta Mech.*, **229**(2), 437-454. https://doi.org/10.1007/s00707-017-1980-7.

Di Matteo, A., Pirrottaa, A. and Tumminelli, S. (2017), “Combining TMD and TLCD: analytical and experimental studies”, *J. Wind Eng. Ind. Aerod.*, **167**, 101-113. https://doi.org/10.1016/j.jweia.2017.04.010.

Diana, G., Resta, F., Sabato, D. and Tomasini, G. (2013), “Development of a methodology for damping of tall buildings motion using TLCD devices”, *Wind Struct*., **17**(6), 629-646. https://doi.org/10.12989/was.2013.17.6.629.

Giaralis, A. and Marian, L. (2016). “Use of inerter devices for weight reduction of tuned mass-dampers for seismic protection of multi-storey buildings: The tuned mass-damperinterter (TMDI)”, *Proceedings of SPIE - The International Society for Optical Engineering*.

Giaralis, A. and Petrini, F. (2017a), “Wind-Induced vibration mitigation in tall buildings using the tuned mass-damper-inerter”, *J. Struct. Eng.*, **143**(9), 04017127. https://doi.org/10.1061/(ASCE)ST.1943-541X.0001863.

Giaralis, A. and Petrini, F. (2017b), “Optimum design of the tuned mass-damper-inerter for serviceability limit state performance in wind-excited tall buildings”, *Procedia Eng.,* **199**, 1773-1778. https://doi.org/10.1016/j.proeng.2017.09.453.

Giaralis, A. and Taflanidis, A.A. (2018), “Optimal tuned mass-damper-inerter (TMDI) design for seismically excited MDOF structures with model uncertainties based on reliability criteria”, *Struct. Control Hlth.*, **25**(2). e2082. https://doi.org/10.1002/stc.2082.

Iban, A.L., Brownjohn, J.M.W., Belver, A.V., Lopez-Reyes, P.M. and Koo, K. (2013), “Numerical modelling for evaluating the TMD performance in an industrial chimney”, *Wind Struct*., **17**(3), 263-274. https://doi.org/10.12989/was.2013.17.3.263.

Karavasilis, T.L., Kerawala, S. and Hale, E. (2012), “Hysteretic model for steel energy dissipation devices and evaluation of a minimal-damage seismic design approach for steel buildings”, *J. Constr. Steel Res.*, **70**, 358-367. https://doi.org/10.1016/j.jcsr.2011.10.010.

Kareem, A., Kijewski, T. and Tamura, Y. (1999), “Mitigation of motions of tall buildings with specific examples of recent applications”, *Wind Struct.,* **2**(3), 201-251.

Kari, L. (1979), “Dynamic vibration absorbers”, *Mech. Engineering publications Ltd*.

Lazar, I.F., Neild, S.A. and Wagg, D.J. (2014), “Using an inerter-based device for structural vibration suppression”, *Earthq. Eng. Struct. Dyn.*, **43**(8), 1129-1147. https://doi.org/10.1002/eqe.2390.

Leung, A., Y.T. and Zhang, H. (2009), “Particle swarm optimization of tuned mass dampers", *Eng. Struct.*, **31**(3), 715-728.

Liang, S., Liu, S., Li, Q.S., Zhang, L. and Gu, M. (2002), "Mathematical model of acrosswind dynamic loads on rectangular tall buildings", *J. Wind Eng. Ind. Aerod.*, **90**(12), 1757-1770. https://doi.org/10.1016/S0167-6105(02)00285-4.

M. Newmark, N. (1959), "A method of computation for structural dynamics", *J. Eng. Mech. Div., ASCE*. **85**(3), 67-94.

Marian, L. and Giaralis, A. (2015), "Optimal design of a novel tuned mass-damper-inerter (TMDI) passive vibration control configuration for stochastically support-excited structural systems", *Probab. Eng. Mech.*, **38**, 156-164. https://doi.org/10.1016/j.probengmech.2014.03.007.

Min, K.W., Kim, H.S., Lee, S.H., Kim, H. and Ahn, S.K. (2005), "Performance evaluation of tuned liquid column dampers for response control of a 76-story benchmark building", *Eng. Struct.*, **27**(7), 1101-111. https://doi.org/10.1016/j.engstruct.2005.02.008.

Ormondroyd, J. and Den Hartog, J.P. (1928), "The theory of dynamic vibration absorber", *T. Amer. Soc. Mech. Eng.*, **50**, 9-22.

Papageorgiou, C. and Smith, M.C. (2006). "Laboratory experimental testing of inerters", *Decision and Control, 2005 and 2005 European Control Conference.*

Poh'Sie, G.H., Chisari, C., Rinaldin, G., Amadio, C. and Fragiacomo, M. (2016), "Optimal design of tuned mass dampers for a multi-storey cross laminated timber building against seismic loads: Optimal design of multiple TMDs used in multi-storey CLT buildings", *Earthq. Eng. Struct. Dyn.*, **45**(12), 1977-1995. https://doi.org/10.1002/eqe.2736.

Poovarodom, N., Kanchanosot, S. and Warnitchai, P. (2001), "Control of man-induced vibrations on a pedestrian bridge bynonlinear multiple tuned mass dampers", *The Eighth East Asia-Pacific Conference on Structural Engineering andConstruction*, Singapore, December.

Poovarodom, N., Kanchanosot, S. and Warnitchai, P. (2003), "Application of non-linear multiple tuned mass dampers to suppress man-induced vibrations of a pedestrian bridge", *Earthq. Eng. Struct. Dyn.*, **32** 1117-1131. https://doi.org/10.1002/eqe.265.

Poovarodom, N., Mekanannapha, C. and Nawakijphaitoon, S. (2002), "Vibration problem identification of steel pedestrianbridges and control measures", *Proceedings of the Third World Conference on Structural Control*, Como, Italy, April.

Rezaee, M. and Aly, A.M. (2016), "Vibration control in wind turbines for performance enhancement: A comparative study", *Wind Struct.*, **22**(1), 107-131. http://dx.doi.org/10.12989/was.2016.22.1.107.

Simiu, E. and Scanlan, R.H. (1986), *Wind effects on structures : an introduction to wind engineering*, Wiley New York.

Spence, S. and Kareem, A. (2013), "Tall buildings and damping: A concept-based data driven model", *J. Struct. Eng.*, **140**(5). https://doi.org/10.1061/(ASCE)ST.1943-541X.0000890.

Ubertini, F. (2010), "Prevention of suspension bridge flutter using multiple tuned mass dampers", *Wind Struct.*, **13**(3), 235-256. https://doi.org/10.12989/was.2010.13.3.235.

Von Kármán, T. (1948), "Progress in the statistical theory of turbulence", *Proceedings of the National Academy of Sciences of the United States of America*, **34**(11), 530.

Wang, Q., Qiao, H., Domenico, D.D., Zhu, Z. and Xie, Z. (2019), "Wind-induced response control of high-rise buildings using inerter-based vibration absorbers", *Appl. Sci.*, **9**(23), 5045. https://doi.org/10.3390/app9235045.

Warburton, G.B. (1982), "Optimum absorber parameters for various combinations of response and excitation parameters", *Earthq. Eng. Struct. Dyn.*, **10**(3), 381-401. https://doi.org/10.1002/eqe.4290100304.

Zhou, X., Lin, Y. and Gu, M. (2015), "Optimization of multiple tuned mass dampers for large-span roof structures subjected to wind loads", *Wind Struct.*, **20**(3), 363-388. https://doi.org/10.12989/was.2015.20.3.363.

Zitzler, E. and Künzli, S. (2004). "Indicator-based selection in multiobjective search", *In International conference on parallel problem solving from nature*. Springer, Berlin, Heidelberg.

TK